

# Search for New Physics in the Exclusive Delayed $\gamma + \cancel{E}_T$ Final State in $p\bar{p}$ collisions at $\sqrt{s} = 1.96$ TeV.

Adam Aurisano  
*Texas A&M University*  
 (Dated: February 8, 2012)

There are a number of models that predict new particles beyond the Standard Model that would produce photons and  $\cancel{E}_T$  in high energy  $p\bar{p}$  collisions. A previous study found preliminary evidence for an excess of photons with delayed arrival times in the  $\gamma + \cancel{E}_T$  final state from  $p\bar{p}$  collisions at  $\sqrt{s} = 1.96$  TeV using the Collider Detector at Fermilab. We propose studying this excess to determine if it arises from mis-estimating backgrounds or from new physics. We examine Standard Model backgrounds to see if there are any biases and find ways to minimize them. Finally, we present a method for estimating background contributions and demonstrate its effectiveness with Monte Carlo samples. The final thesis will complete these studies and answer the question, within capabilities, whether this excess can be explained by known background sources.

## INTRODUCTION

The Standard Model (SM) describes all currently known particles and interactions relevant at energies levels accessible in current collider experiments [1]. The SM has enjoyed tremendous success since its inception, and all particles it predicts have been found except for the Higgs particle. The Higgs particle breaks the symmetry that the SM posits between electromagnetism and the weak force, so it (or something like it) is necessary for the validity of the SM. However, the Higgs particle is also one of the reasons why the SM is not believed to be a complete description of reality.

The following discussion about the Higgs and Supersymmetry derives from [2]. All particles have quantum mechanical corrections to their mass in quantum field theory; however, the Higgs particle accumulates corrections of a particularly difficult kind. For instance, for a fermion that couples to the Higgs with strength  $\lambda_f$ , the leading correction to the Higgs mass from that fermion is  $\Delta m_H^2 = -\frac{|\lambda_f|^2}{8\pi^2} \Lambda_{UV}^2$  where  $\Lambda_{UV}$  is the ultraviolet cut-off scale. The ultraviolet cutoff allows the calculation to be finite and is assumed to come from new physics at a higher scale. If that scale is the Planck scale, the energy at which gravity is thought to become important quantum mechanically, the Higgs mass is 30 orders of magnitude bigger than what is consistent with what has already been observed. The fact that the Planck scale is so large compared to the electroweak scale is known as the “hierarchy problem”. Since the Planck scale cannot provide the ultraviolet cutoff, there are a few options for making the Higgs mass corrections work. One option is for the role of the Higgs to be played by composite particles [3]. Another is for some other new physics to enter at a lower scale to provide the ultraviolet cutoff. The last is that some new physics exists that causes a cancellation of terms in the Higgs mass correction.

Supersymmetry (SUSY) has been shown to be very

powerful in solving a number of important problems in particle physics, cosmology, and string theory. Among these is the “hierarchy problem” [2, 4]. In the quantum mechanical mass corrections, terms due to virtual boson loops and virtual fermion loops have opposite signs. SUSY posits a symmetry such that every fermion has a bosonic partner (and vice-versa). This symmetry causes the bosonic and fermionic terms in the Higgs mass corrections to approximately cancel. The model containing the minimal set of new SUSY particles is called the minimal supersymmetric Standard Model (MSSM). In the MSSM quarks and leptons have spin-0 partners called squarks ( $\tilde{q}$ ) and sleptons ( $\tilde{l}$ ). Gluons have spin-1/2 partners called gluinos ( $\tilde{g}$ ). The Higgs sector becomes more complicated in SUSY. Instead of a single particle, there must be two Higgs chiral supermultiplets which leads to 4 physical scalar particles ( $H^\pm$ ,  $h_0$ , and  $H_0$ ) and one physical pseudoscalar ( $A_0$ ). This is necessary to prevent a gauge anomaly in the electroweak gauge symmetry. The partners of the Higgs particles and the gauge bosons ( $Z_0$ ,  $W^\pm$ , and  $\gamma$ ) are spin-1/2. Of these, the charged particles mix to produce charginos ( $\tilde{\chi}_i^\pm$ ) and the neutral particles mix to produce neutralinos ( $\tilde{\chi}_i^0$ ). In some models, the graviton is included. In those models, its partner is the spin-3/2 gravitino ( $\tilde{G}$ ).

Unfortunately, for the cancellation of the Higgs mass divergence to be exact, the new supersymmetric partners would have to have the same mass as their SM counterparts. Since this is not observed, one must break the symmetry “softly” such that there are no quadratic divergences in the mass corrections for the Higgs particles to maintain the advantages of SUSY. Supersymmetry breaking occurs in a hidden sector which has little direct coupling to the visible MSSM sector. This breaking is communicated from the hidden to the visible sector by some mediating interaction. Depending on the nature of the mediating interactions, the phenomenology of the resulting model changes. Several su-

persymmetry breaking schemes exist such as: Supergravity (SUGRA) [5], Anomaly Mediated Supersymmetry Breaking (AMSB) [6] and Gauge Mediated Supersymmetry breaking (GMSB) [7].

We focus on GMSB because, in addition to its theoretical advantages (such as suppressing flavor-changing), it has a phenomenology that makes it particularly interesting to search for. In GMSB new messenger particles link the supersymmetry breaking vacuum expectation value  $\langle F \rangle$  and the MSSM by means of ordinary gauge interactions. Unlike other models, the lightest supersymmetric particle (LSP) is the gravitino. Generally speaking, if  $\tilde{X}$  is the next-to-lightest supersymmetric particle (NLSP) and  $\sqrt{\langle F \rangle}$  is less than a few TeV, the lifetime of  $\tilde{X}$  decaying via the interaction  $\tilde{X} \rightarrow X + \tilde{G}$  can be small enough to occur on the scale of a detector but large enough to be measured. In particular if  $\tilde{\chi}_1^0$  is the NLSP, it can have a lifetime on the order of nanoseconds before decaying via  $\tilde{\chi}_1^0 \rightarrow \gamma + \tilde{G}$ .

In the most general version of GMSB, general gauge mediation (GGM), it is possible for  $\tilde{G}$  have a mass less than  $1 \text{ keV}/c^2$  and  $\tilde{\chi}_1^0$  have a mass less than  $50 \text{ GeV}/c^2$ . Because  $M_{\tilde{\chi}_1^0}$  is less than  $M_{Z^0}$ , the branching ratio of  $\tilde{\chi}_1^0 \rightarrow \gamma + \tilde{G}$  is almost 100%. It has been shown [8] that if  $\tilde{\chi}_1^0$  and  $\tilde{G}$  are the only accessible particles, current experimental limits on GMSB do not apply. Instead of cascade decays typical of minimal GMSB scenarios with SPS-8 relations [9], direct supersymmetric particle production is essentially zero. Furthermore, if  $2M_{\tilde{\chi}_1^0} < M_{h^0}$  the branching ratio of  $h^0 \rightarrow \tilde{\chi}_1^0 \tilde{\chi}_1^0$  can become large. In the production shown in Fig. 1, the  $\tilde{\chi}_1^0$  is producible at the Fermilabe Tevatron and is long-lived, so frequently only one decays inside the detector. In addition, the  $\tilde{G}$  leave the detector without interacting, so the final state is  $\gamma + \cancel{E}_T$ . As shown in Fig. 2, the path length travelled by  $\tilde{\chi}_1^0$  before it decays is long enough that the  $\gamma$  is delayed, that is, it is detected later than expected if it have been produced promptly (directly from the interaction point). This gives rise to the exclusive delayed  $\gamma + \cancel{E}_T$  final state we will study.

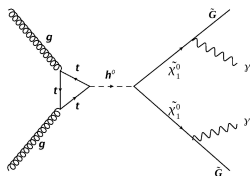


FIG. 1. The dominant sparticle production mechanism assuming that all sparticles other than the  $\tilde{\chi}_1^0$  and the gravitino are too heavy to be produced at the Tevatron, and  $M_{h^0} \gtrsim 2M_{\tilde{\chi}_1^0}$ .

A preliminary study [10] found an excess of delayed photons in the  $\gamma + \cancel{E}_T$  exclusive final state using crude

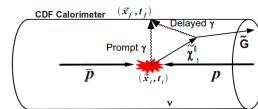


FIG. 2. Schematic of a  $t_{corr}$  measurement. The  $t_{corr}$  measurement is designed to yield zero in the case of a prompt photon. In the case of a photon resulting from the decay of a long-lived  $\tilde{\chi}_1^0$ , the extra path length relative to prompt expectation produces a delayed time.

background estimation techniques. In this thesis we add significantly more data, develop new requirements to minimize bias, and perform a proper background estimation.

## EXPERIMENTAL SETUP

We will perform this analysis at the Tevatron collider at Fermilab. Recently shutdown, the Tevatron is a proton-antiproton superconducting synchrotron with a 1 km radius and a center of mass energy of  $\sqrt{s} = 1.96 \text{ TeV}$  [11]. Protons and anti-protons collected into 36 bunches counter-rotate in a single ring. Every 396 ns collisions occur at two beam crossing points where the two multi-purpose detectors, CDF II and D0 are located. By shutdown the Tevatron delivered  $\sim 12 \text{ fb}^{-1}$  of integrated luminosity. CDF II [12] and D0 each recorded approximately  $10 \text{ fb}^{-1}$  of integrated luminosity. The transverse, longitudinal, and time profile of the beam at the interaction points are approximately Gaussian. The transverse width is  $\sim 30 \text{ cm}$ , the longitudinal width is  $\sim 30 \text{ } \mu\text{m}$ , and the time width is  $\sim 1.28 \text{ ns}$ .

We will use  $\sim 6.3 \text{ fb}^{-1}$  of data collected from Tevatron collisions collected by the CDF II detector [12] for this analysis. To describe our experiment, we use a cylindrical coordinate system where the  $z$  axis is along the beam line in the direction of the proton beam,  $\theta$  is the polar angle relative to the proton beam direction,  $\phi$  is the azimuthal angle, and  $\eta = -\ln \tan(\theta/2)$ . In addition, we define  $E_T = E \sin\theta$ ,  $P_T = P \sin\theta$ , and  $\cancel{E}_T$  is the magnitude of  $\vec{\cancel{E}}_T = -\sum_i E_i \vec{n}_i$  where  $E_i$  is the energy of the  $i^{\text{th}}$  calorimeter tower and  $\vec{n}_i$  is the unit vector from the interaction point to the  $i^{\text{th}}$  calorimeter tower in the  $x-y$  plane.

The inner most portion of the CDF detector is composed of tracking chambers sitting inside a 1.4 T superconducting solenoid which allows the measurement of momentum for charged particles. The silicon vertex detector (SVX II) [13] is close to the beam pipe and is composed of both stereo and axial microstrips. Further from the beam line is the central outer tracker (COT) [14] which is a multiwire drift chamber. The COT is composed of 4 axial and 4 stereo superlayers with 12 layers each. In addition to measuring  $z$  and  $\phi$ , the COT outputs times

which can be used to determine the originating time of a charged particle. Tracks with enough COT hits to have a reconstructed initial time can be clustered by both the fitted originating  $z$  and time (space-time vertexing). This allows us to extrapolate back to reconstruct the time and position of the collision producing the observed particles.

Outside of the solenoid, there are calorimeters to measure particle energies. Within  $|\eta| < 1.1$  is the central electromagnetic calorimeter (CEM) [15], which measures the energies of electromagnetically interacting particles, such as photons and electrons, using lead-scintillator sampling. It is segmented in towers of 15 degrees in  $\phi$  and 0.1 in  $\eta$  and has a radiation depth of 18 radiation lengths to fully contain the shower of electromagnetic particles. Embedded inside CEM towers at the expected shower maximum is the central electromagnetic shower-max (CES). It is composed of orthogonal strips and wires, which allow a precision measurement of the shower's  $z$  and  $\phi$ . Particles which deposit at least  $\sim 3$  GeV in the CEM can have their arrival time measured by the EMTiming system [16]. This system has been shown to have an intrinsic resolution of  $\sim 0.59$  ns.

## OVERVIEW OF THE ANALYSIS

The previous study [10] searched in the exclusive  $\gamma + \cancel{E}_T$  final state defined in Table I. We continue to use these cuts as a baseline for the analysis; however, we will modify these requirements to reduce backgrounds and biases. The backgrounds to this final state are shown in Table II. The dominant backgrounds are from  $W \rightarrow e\nu \rightarrow \gamma_{fake} + \cancel{E}_T$ ,  $\gamma + jet \rightarrow \gamma + jet_{lost} \rightarrow \gamma + \cancel{E}_T$ ,  $Z\gamma \rightarrow \nu\nu\gamma \rightarrow \gamma + \cancel{E}_T$ , and cosmic rays.

Reconstructed $\gamma$ with $E_T > 45$ GeV and $ \eta  < 1.1$
$\cancel{E}_T > 45$ GeV
No reconstructed track with $P_T > 10$ GeV
No reconstructed calorimeter cluster with $E_T > 15$ GeV

TABLE I. Baseline selection requirements to identify events in the exclusive  $\gamma + \cancel{E}_T$  final state.

$W \rightarrow e\nu \rightarrow \gamma_{fake} + \cancel{E}_T$
$W \rightarrow \tau\nu \rightarrow \gamma_{fake} + \cancel{E}_T$
$W\gamma \rightarrow l\nu\gamma \rightarrow l_{lost} + \gamma + \cancel{E}_T$
$\gamma + jet \rightarrow \gamma + \cancel{E}_T_{fake}$
$Z\gamma \rightarrow \nu\nu\gamma \rightarrow \gamma + \cancel{E}_T$
Cosmic Rays
Beam Halo
Satellite Bunches

TABLE II. Backgrounds in the exclusive  $\gamma + \cancel{E}_T$  final state.

The primary signal we are looking for can be modeled using the production of a heavy, neutral particle which

travels for a few nanoseconds before decaying into a photon and a particle that does not interact in the detector, as shown in Fig. 2. As shown in Ref. [17], the most powerful way to separate these events is to look for photons which arrive at the detector with a time that is delayed relative to expectations. To quantify this, we define the corrected time as the measured time of arrival of the photon at the electromagnetic calorimeter relative to the expectations for a photon emitted from the initial collision, that is

$$t_{corr} \equiv (t_f - t_i) - \frac{|\vec{x}_f - \vec{x}_i|}{c}, \quad (1)$$

where  $t_f$  is the time of arrival at the electromagnetic calorimeter as measured by the EMTiming system,  $\vec{x}_f$  is the point of arrival at the calorimeter taken from the CES cluster associated with the photon object, and  $t_i$  and  $\vec{x}_i$  are the time and place where the photon was produced taken from the space-time vertex associated with the event.

There are several scenarios which yield distinctive  $t_{corr}$  distributions. If the photon is “prompt”, that is, the photon comes directly from collision, and we select the correct space-time vertex,  $t_{corr}$  should be zero up to experimental resolution. The resolution for these “right vertex” events is approximately 0.64 ns. The right-vertex distribution of  $W \rightarrow e\nu$  electron data, where using the fact that electrons look like photons in the calorimeter and ignoring the electron track in the vertexing allows us to approximate  $\gamma + \cancel{E}_T$ , is shown in Fig. 3.

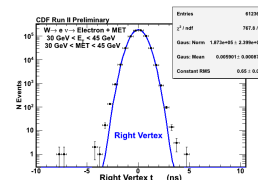


FIG. 3. If the reconstructed vertex with the highest  $\Sigma P_T$  is the origin of the detected photon or electron, the event is classified as “right vertex”. Right-vertex events have a mean of  $\sim 0$  ns and an RMS of  $\sim 0.64$  ns.

Because photons have no charge, there is no track associated with them to assist us in picking the right vertex. We select the reconstructed space-time vertex with the highest  $\Sigma P_T$  as the presumed origin of the photon. If this is not true because an unrelated collision had higher  $\Sigma P_T$  or because the collision did not produce a vertex, the time of flight and vertex time subtracted in the  $t_{corr}$  calculation are no longer related to the actual time of flight and origin time of the photon. The width of the  $t_{corr}$  distribution of these “wrong vertex” increases to  $\sim 2.0$  ns due to the transverse and time profile of the beam. The wrong vertex distribution of  $W \rightarrow e\nu$  electron data is shown in Fig. 4. The mean of the wrong-vertex distribution was previously assumed to be zero [10, 17], but we

now know that this is not generally true.

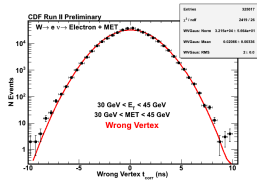


FIG. 4. If the reconstructed vertex with the highest  $\Sigma P_T$  is not the origin of the detected photon or electron, the event is classified as “wrong vertex”. Wrong-vertex events have an RMS of  $\sim 2.0$  ns, and they may or may not have a mean at 0 ns.

Heavy, neutral, long-lived particles decaying to photons, like a long-lived  $\tilde{\chi}_1^0$ , produce a distinctively delayed distribution. As shown in Fig. 2, since the photon comes from a displaced decay, the path length travelled by the  $\tilde{\chi}_1^0$  in addition to the photon is generally longer than that of a prompt photon. Since the decay time of the  $\tilde{\chi}_1^0$  is exponentially distributed with a mean time of  $\tau$ ,  $t_{corr}$  is also exponentially distributed up to the  $t_{corr}$  resolution (here assumed to be the right-vertex RMS of 0.64 ns). However, the mean  $t_{corr}$  is typically not the same as  $\tau$  due to the masses of the  $h_0$  and  $\tilde{\chi}_1^0$  and their decay distributions. An example of the signal distribution is shown in Fig. 5.

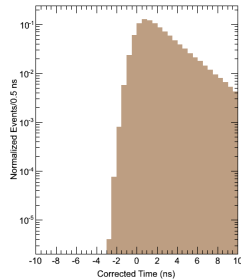


FIG. 5. The  $t_{corr}$  timing distribution for photons produced by heavy, neutral, long-lived particles is an exponential smeared by EMTiming resolution. This distribution has decay constant of 2.5 ns and is smeared by 0.65 ns. We expect a decay constant of 2.5 ns for the benchmark GMSB point with  $M(h^0) = 135$  GeV,  $M(\tilde{\chi}_1^0) = 65$  GeV, and  $\tau(\tilde{\chi}_1^0) = 5$  ns.

In addition to Standard Model backgrounds, reconstructed photons due to cosmic rays striking the detector are a large background source. Since cosmic rays are completely uncorrelated with the collision, they appear flat in time. In Fig. 6, we can see that data selected to be rich in cosmic rays is roughly flat for most of the energy integration window around the collision. Near the opening and closing of the energy integration window the rates decrease due not all of the energy being captured within the window.

To separate out right vertex, wrong vertex, and cos-

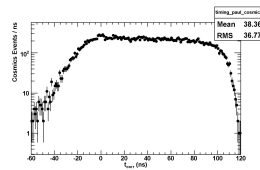


FIG. 6. An example of cosmic rays in data. Cosmic rays pass through the detector at a constant rate, and they are uncorrelated with the collision. Away from the edges of the energy integration window, cosmics are approximately flat in time.

mic ray events, we define four timing regions: the control region (CR) with  $-7ns > t_{corr} > -2ns$ , the bulk region (BR) with  $-2ns > t_{corr} > 2ns$ , the signal region (SR) with  $2ns > t_{corr} > 7ns$ , and the cosmics region with  $20ns > t_{corr} > 80ns$ . These regions are shown in Fig. 7. The control region contains mostly cosmics and wrong-vertex events. The bulk region contains mostly right-vertex events. The signal region contains mostly cosmics and wrong-vertex events, but if signal is present, it would be predominantly in this region. The cosmics region is both away from the regions dominated by real collision and the edge of the integration window, so it is almost entirely cosmics. We use this region to estimate the cosmics rate to extrapolate back into the collision dominated regions. This will be our largest background, but it will have a small uncertainty.

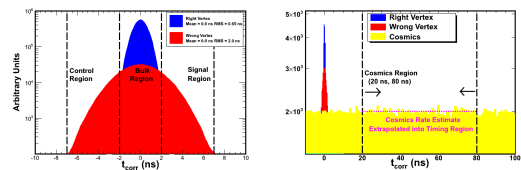


FIG. 7. (a) The  $t_{corr}$  timing distribution is described by a right vertex Gaussian, a wrong vertex Gaussian, and flat cosmics. The control region contains mostly wrong vertex and cosmic events, the bulk region contains mostly right vertex events, and the signal region contains mostly wrong vertex and cosmic events. If there are delayed photons, they would appear in the signal region. If the wrong-vertex mean were zero, the signal region background prediction could be estimated from the control region. This is not generally true. (b) Because cosmic ray events are flat in time, we can estimate their rate using the cosmics region. This region is a pure cosmics sample.

In previous delayed photon analyses [10, 17], with a small fraction of the data, the wrong-vertex distribution was always assumed to be symmetric about zero. This was not a bad strategy because the fraction of events that were wrong vertex was very small. If the wrong-vertex distribution had a mean of zero, we could estimate the background expectations in the signal region as being equal to the observed number of events in the control region. The timing distribution from the previous exclu-

sive  $\gamma + \cancel{E}_T$  analysis that motivated this search with the old background estimate is shown in Fig. 8. Using this method, there is an extremely large excess in the signal region. Since extraordinary claims require extraordinary evidence, we have sought to understand if SM physics or detector effects could create such a large excess.

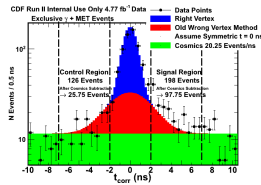


FIG. 8. This shows the results of a previous analysis in the exclusive  $\gamma + \cancel{E}_T$  final state. Using a background estimation assuming the wrong vertex mean is zero leads to a large apparent excess.

We have uncovered a number of effects that cause the wrong-vertex mean not to be zero, and, therefore, invalidate old background estimate for the exclusive  $\gamma + \cancel{E}_T$  final state. We found that biases can come from mis-measuring photon  $E_T$  due to selecting the wrong vertex, electrons being mis-identified as photons, and jets being lost.

First, because  $E_T \equiv E \sin \theta$ , and  $\theta$  is measured relative to the  $z$  position of the reconstructed vertex, we mis-measure  $E_T$  if we select the wrong vertex. As shown in Fig. 9, the mis-measurement of  $E_T$  and  $t_{corr}$  due to selecting the wrong vertex are correlated. If the  $E_T$  increases due to selecting the wrong vertex, the  $t_{corr}$  also increases on average. Similarly, if  $E_T$  decreases due to selecting the wrong vertex, the  $t_{corr}$  decreases on average. If events that have a true  $E_T$  below our requirement of 45 GeV enter our sample due to being promoted in from selecting the wrong vertex, that increases that average time of the events in our sample. If events have a true  $E_T$  above our requirement but they exit our sample due to being demoted out from selecting the wrong vertex, that also increases the average time of the events in our sample by removing events that tend to have negative times. This “threshold effect” is particularly important in exclusive  $\gamma + \cancel{E}_T$  events coming from  $W \rightarrow e\nu \rightarrow \gamma_{fake} + \cancel{E}_T$  due to many events having a true  $E_T$  near the 45 GeV threshold. We partially decouple the  $E_T$  and  $t_{corr}$  measurements by recalculating  $E_T$  and  $\cancel{E}_T$  relative to a  $z$  other than the reconstructed vertex.

A second effect we uncovered is that electrons mis-identified as photons tend to have larger mean wrong-vertex times than a similar sample of properly identified electrons or properly identified photons. Electrons that are mis-identified as photons typically have a longer path length than properly identified electrons or photons. This is because the probability of an electron radiating away most of its energy as a photon increase as it travels through more material. The locations of such radiation

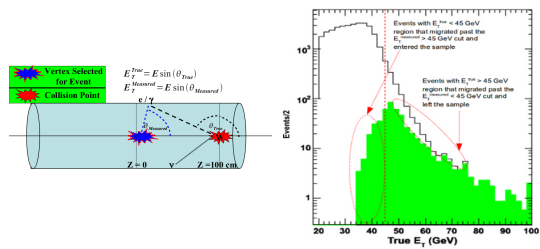


FIG. 9. (a) A cartoon showing the correlation in the mis-measurement of  $E_T$  and  $t_{corr}$  due to selecting the wrong vertex. (b) The true  $E_T$  of exclusive  $\gamma + \cancel{E}_T$  events in  $W \rightarrow e\nu$  Monte Carlo. The events promoting over threshold into the sample and those demoting out of the sample create a net positive shift in the wrong-vertex mean.

events in  $w \rightarrow e\nu$  Monte Carlo is shown in Fig. 10. The fact that most of such radiation events occur inside the SVX suggests a strategy for reducing the number of mis-identified electrons in our sample. Instead of rejecting reconstructed photons with a track which extrapolates to close to the CES cluster (as is normally done), we reject reconstructed photons which are close to a track relative to its initial  $\eta$  and  $\phi$ .

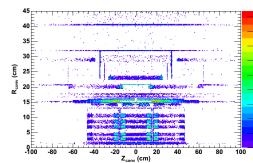


FIG. 10. The location of radiation events where an electron radiated away a photon with at least half of the original energy in exclusive  $\gamma + \cancel{E}_T$  events from  $W \rightarrow e\nu$  Monte Carlo. The structures below 10 cm are the layers of the SVX. Most radiation events occur  $\sim 15$  cm which corresponds to the port cards which read out data from the SVX.

Finally, we normally only consider vertices within the “luminous region”, that is,  $|z| < 60$  cm. If a background event were produced with at a  $z$  outside of the luminous region, the mean wrong-vertex time could be quite shifted as the path length is almost always measured to be smaller than the true path length. As shown in Fig. 11, exclusive  $\gamma + \cancel{E}_T$  events coming from QCD  $\gamma + jet$  production have a large number of events produced at extreme positions. This results from the fact that to enter the exclusive  $\gamma + \cancel{E}_T$  sample, the jet must fail to be reconstructed. There are limited ways that this can happen. Either the jet is very low energy, it travels through an uninstrumented portion of the detector, or it is produced pointing out of the detector. In the latter case, the collision must occur at  $|Z| > 60$  cm so the jet exits the detector without interacting. To reduce this background, we require that there be no reconstructed vertices outside the luminous region.

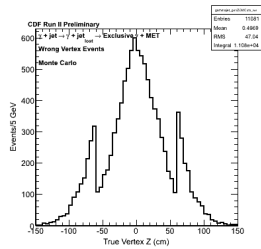


FIG. 11. The true collision position of exclusive  $\gamma + \cancel{E}_T$  events from  $\gamma + jet$  Monte Carlo. There is a sharp increase in events originating outside of the luminous region.

## ANALYSIS STRATEGY

Given that it is clear that the wrong-vertex mean is not zero in the exclusive  $\gamma + \cancel{E}_T$  sample, we need a new strategy to estimate the background contributions in the signal region. Although the control and bulk regions contain some information about the wrong-vertex distribution, the presence of cosmics and right-vertex events typically make it very hard to extract; moreover, number of wrong-vertex events in the control region decreases as the wrong-vertex mean increases. To solve this problem, we look at those events which would have been in the exclusive  $\gamma + \cancel{E}_T$  sample aside from having no reconstructed vertex in the luminous region. We call this the no-vertex sample, and we can define a no-vertex photon time by assuming a vertex with  $z = 0$  and  $t = 0$ . This distribution is approximately Gaussian and has an RMS of  $\sim 1.6$  ns which comes from intrinsic EMTiming resolution and the beam profile [17]. Using multiple Monte Carlo samples, we find that the mean of the no-vertex distribution and the mean of the wrong-vertex distribution should not be more than 40 ps different, and is often less. In Fig. 12 we see that in real data and a variety of Monte Carlo sample with a full simulation, the mean no-vertex time and the mean wrong-vertex time are consistent with each other well within a 100 ps systematic uncertainty. Using information from the no-vertex distribution in combination with normal exclusive  $\gamma + \cancel{E}_T$  sample makes estimating the wrong-vertex mean possible.

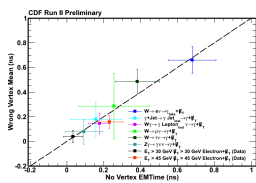


FIG. 12. The wrong-vertex mean vs. the no-vertex mean raw time for various Monte Carlo and data samples. The wrong-vertex mean and the no-vertex mean raw time are consistent with each other up to a 100 ps systematic uncertainty.

We know that each SM background contributes a

right-vertex distribution and a wrong-vertex distribution which are both approximately Gaussian. However, several SM backgrounds contribute to the exclusive  $\gamma + \cancel{E}_T$  final state, and each of these backgrounds has a different characteristic wrong-vertex mean. While the difference between the means is small compared to the expected wrong-vertex RMS of 2.0 ns, it is important to determine if it is possible to approximate the combined SM backgrounds as a double Gaussian. To determine this, we consider the two SM background with the largest difference in wrong-vertex means in Monte Carlo:  $W \rightarrow e\nu$  with a wrong-vertex mean of  $\sim 0.6$  ns and  $Z\gamma \rightarrow \nu\nu\gamma$  with a wrong-vertex mean of  $\sim 0$  ns. We generate toy Monte Carlo wrong vertex distributions with these two means, and we combine them in various fractions. In Fig. 13 we see the results of fitting the combined distributions to a Gaussian in the control and bulk regions. We find that fitted mean is simply weighted mean of the two combined datasets. The fitted RMS increases as we move to combining equally sized Gaussians. We see that a 5% uncertainty in the RMSs of the wrong and no vertex distributions covers the variation in the fitted Gaussian due to combining backgrounds.

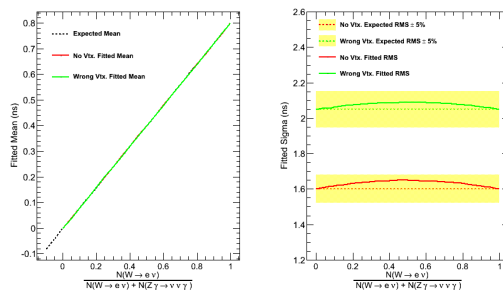


FIG. 13. The effect on the measured mean and RMS of the wrong-vertex distribution in a toy Monte Carlo where we combine in various fractions two Gaussians modeling the two Monte Carlo backgrounds with the largest difference between their means,  $W \rightarrow e\nu$  and  $Z\gamma \rightarrow \nu\nu\gamma$ .

To make our full background estimate, we construct a combined, extended likelihood function for the final data sample where we have separated events into two categories: ones with a good reconstructed vertex and ones with no vertex. We incorporate systematic uncertainties as Gaussian constraints [18] shown in Table III. We maximize this likelihood function and integrate the predicted good-vertex distribution in (2,7) ns to estimate the number of events in the signal region. The fit uncertainties, which combine statistical and systematic uncertainties, can be straight-forwardly propagated to estimate of the number of events in the signal region.

To validate this method, we take fully reconstructed Monte Carlo samples of the three significant SM backgrounds with wrong-vertex means that span the expected mean in data (0.0 ns, 0.2 ns, 0.4 ns),  $W \rightarrow e\nu$ ,  $Z\gamma \rightarrow \nu\nu\gamma$ ,

and  $\gamma + jet$ , and we sample them to create pseudo-experiments. We draw a number of events consistent with our expectations in data, and we sample from the three Monte Carlo sets in random fractions. We then add a flat distribution to approximate the cosmic ray contribution to each pseudo-experiment. This allows us to test the fitting method with a spectrum of wrong-vertex means. In addition, this tests our assertion that the combination of backgrounds can be approximated by a double Gaussian. For each pseudo-experiment, we maximize the likelihood and calculate  $\frac{N(SR)_{Obs} - N(SR)_{Exp}}{\sqrt{N(SR)_{Obs} + \sigma_{fit}^2}}$ , a measure of the significance of any observed excess. In the absence of a real excess (as in SM Monte Carlo) this quantity ought to be Gaussian distributed with a mean of 0 and an RMS of 1. The distribution of this quantity for the pseudo-experiments is shown in Fig. 14. The mean of the distribution is very close to zero, as expected, and indicates that the method has little bias. The RMS of the distribution being close to one indicates that the uncertainties are well estimated. Indeed, it is slightly less than one, indicating that our systematic uncertainties assume a larger variation than that observed in our fully simulated Monte Carlo samples.

Right-Vertex Mean = $0.0 \pm 0.1$ ns
Right-Vertex RMS = $0.64 \pm 0.1$ ns
Wrong-Vertex Mean = No-Vertex Mean $\pm 0.1$ ns
Wrong-Vertex RMS = $2.0 \pm 0.1$ ns
No-Vertex RMS = $1.6 \pm 0.1$ ns

TABLE III. Gaussian constraints added to the combined, extended likelihood function to incorporate systematic uncertainties.

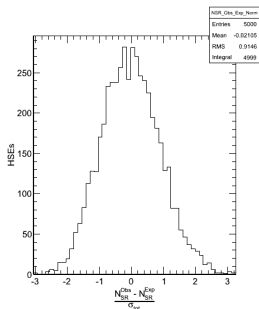


FIG. 14. A validation of the fit method. We draw pseudo-experiments of approximately the statistics level expected in data by sampling Monte Carlo events from the three most significant SM backgrounds,  $W \rightarrow e\nu$ ,  $Z\gamma \rightarrow \nu\nu\gamma$ , and  $\gamma + jet$ , in random fractions. In addition, we add a flat cosmic background to the good vertex distribution and no vertex distribution. This figure shows that the prediction for the number of events in the signal region has little bias, and the estimated uncertainty accurately describes the variation in fit results.

## CONCLUSIONS

A preliminary study in the exclusive  $\gamma + \cancel{E}_T$  final state showed a large excess which could have indicated the presence of  $\tilde{\chi}_1^0 \rightarrow \gamma_{delayed} \tilde{G}$  decays in the general gauge mediated supersymmetry breaking context [8, 10]. We set out to examine all the assumptions of the preliminary study to determine if more mundane physics could account for the excess. Our preliminary results indicate that the excess shown in Fig. 8 is not robust. Much of the excess is due to highly biased Standard Model events. Similarly, the background estimate was significantly underestimated by assuming a wrong vertex mean of zero. Our primary goal for this thesis is a full and proper analysis of the backgrounds in the signal region to see if any excess persists.

- 
- [1] D. Perkins, *Introduction to High Energy Physics*, 4th ed. (Cambridge University Press, New York, NY, 1988); F. Halzen and A. D. Martin, *Quarks and Leptons* (John Wiley and Sons, New York, NY, 1984); C. Quigg, *Gauge Theories of the Strong, Weak, and Electromagnetic Interactions* (Addison-Wesley, Reading, MA, 1983).
  - [2] S. Martin, (1997), arXiv:hep-ph/9709356.
  - [3] K. Lane, (1994), arXiv:hep-ph/9401324v2; S. Martin, Phys. Rev. **D 46**, 2192 (1992), arXiv:hep-ph/9204204v2; M. Schmaltz and D. Tucker-Smith, Ann.Rev.Nucl.Part.Sci. **55**, 229 (2005), arXiv:hep-ph/0502182v1.
  - [4] C. Kolda and H. Murayama, JHEP **07**, 035 (2000), arXiv:hep-ph/0003170.
  - [5] R. Arnowitt and P. Nath, (1997), arXiv:hep-ph/9708254.
  - [6] F. Paige and J. Wells, (2000), arXiv:hep-ph/0001249.
  - [7] C. Kolda, Nucl.Phys.Proc.Suppl. , 266 (1998), arXiv:hep-ph/9707450.
  - [8] J. D. Mason and D. Toback, Phys. Lett. **B 702**, 377 (2011).
  - [9] B. Allanach *et al.*, The European Physical Journal C - Particles and Fields **25**, 113 (2002), 10.1007/s10052-002-0949-3.
  - [10] M. Goncharov, private communication (2008).
  - [11] D. Acosta *et al.* (CDF Collaboration), Phys. Rev. **D 71**, 032001 (2005).
  - [12] F. Abe *et al.*, FERMILAB-Pub-96/390-E CDF 6261.
  - [13] A. Sill *et al.*, Nucl. Instrum. Meth. **A447**, 1 (2000).
  - [14] T. Affolder *et al.*, Nucl. Instrum. Meth. **A526**, 249 (2004).
  - [15] L. Balka *et al.*, Nucl. Instrum. Meth. **A267**, 272 (1988).
  - [16] M. Goncharov *et al.*, Nucl. Instrum. Meth. **A565**, 543 (2006).
  - [17] D. Toback and P. Wagner, Phys. Rev. **D 70**, 114032 (2004), arXiv:hep-ph/0407022v1; A. Abulencia *et al.* (CDF Collaboration), Phys. Rev. Lett. **99**, 121801 (2007); T. Aaltonen *et al.* (CDF Collaboration), Phys. Rev. **D 78**, 032015 (2008).
  - [18] J. Conway, (2011), arXiv:1103.0354v1.